Identifying Defects and Their Electronic Signatures at Regrown GaN Junctions

J. He,[1] G. Cheng,[1] A. Zimmerman,[1] S. Frisone,[1] F. Naab,[2] M. Nami,[3] B. Li,[3] J. Han,[3] R. S. Goldman[1*]

[1]*Department of Materials Science and Engineering, University of Michigan, Ann Arbor, Michigan 48109-2136, USA*

[2] *Michigan Ion Beam Laboratory, University of Michigan, Ann Arbor, Michigan 48109, USA*

[3] *School of Engineering and Applied Science, Yale University, New Haven, Connecticut 06520-8292, USA*

May 2, 2021

ABSTRACT

We have investigated the influence of the ambient exposure and/or ICP etching on the structure and properties of GaN p-i-n structures for high power electronics. To quantify the concentration of various native and extrinsic point defects, we utilize a combination of ion beam analyses in conjunction with x-ray diffraction. The full width at half max (FWHM) of phi and omega scans were used to quantify the mosaicity and threading dislocation (TD) densities at the p-i interfaces. The lowest densities of *c*-type and highest densities *a*-type TD components are observed for the "in-situ" GaN structure, which also produces the highest interfacial donor-acceptor pair (DAP) cathodoluminescence (CL) emissions. Interestingly, elastic recoil detection analysis (ERDA) and Rutherford backscattering spectroscopy reveal the lowest interfacial [H] but the highest fraction of displaced Ga atoms, suggesting efficient incorporation of Mg_{Ga} in the in-situ structure. On the other hand, for the ex-situ structures, minimal interfacial [H] is also observed, but the lowest interfacial NBE and DAP CL emission is apparent as well as the highest density of

c-type TD components. The relationship between interfacial [H], displaced Ga, CL emission features, and *c*- and *a*-type dislocation densities will be discussed.

*Corresponding Author: rsgold@umich.edu

Although silicon-based electronics are used to power light-emitting diodes and electric vehicles, their utility in high power applications is limited by slow switching and high on-state resistance. The most promising alternative power devices consist of vertical GaN devices. Although vertical GaN devices exhibit promising performance for high power applications, [1,2] their commercialization has been limited by several obstacles. To date, most vertical GaN power devices have been fabricated on free-standing GaN substrates, whose cost per unit area exceeds that of silicon substrates by a factor of 1000.[3] In addition, GaN substrates further increase the costs in the epitaxial film growth due to their small diameter.

An additional requirement for vertical high power GaN devices is a viable selective-area doping approach that yields high quality p-n junctions.[4] Although selective-area doping techniques including masked ion-implantation and/or dopant diffusion have been explored, [5,6] they are limited to shallow junction formation and require high temperature annealing. To date, both inductively-coupled plasma (ICP) etching and pulsed photo-electrochemical (PEC) etching, have been used to achieve selective-area Mg-doping of GaN. Cathodoluminescence spectroscopy reveals non-uniform Mg distributions for the ICP-etched GaN mesa structure. [7] Photoluminescence spectroscopy reveals a reduction in surface/interface damage for GaN mesas prepared by pulsed PEC etching in comparison with those prepared by ICP etching, but bumps around dislocations are also reported.[8] Though recovery from plasma-induced damage has also been reported using

rapid thermal annealing and wet potassium hydroxide etching,[9] creation of damage-free regrowth interface is still in progress.[4] A promising approach for high quality p-n junctions is selective-area etching followed by selective-area regrowth.[6] However, to fully develop this approach, a detailed understanding of the influence of dry etching and metal-organic surface preparation on the structure and properties of the ICP-etched/regrown interface is critical. For example, though solvent cleaning is found to incorporate significant Si impurities at the regrowth interface, no research on Si impurities incorporation in the process that involved etching followed by solvent cleaning during the regrowth has been done.[10] At the same time, previous studies of IV characteristics and the electron signatures correlated Si impurities to the leakage current, but simultaneous investigation of structural crystallinity, Si, H impurities, and their electronic signature has not yet been performed.[11]

Ion beam analysis techniques, including RBS/c and ERDA, have been used to quantitatively determine composition, uniformity, impurity, and elemental depth profiles of major, minor, and trace elements in GaN.[12] To date, RBS/c studies of GaN/sapphire,[13] GaN bulk,[14] and implanted GaN bulk,[15] have revealed minimum values ranging from 1.2% to 4%; but RBS/c studies of GaN homoepitaxy have not been reported. ERDA studies of Mg ion implanted GaN bulk have revealed Mg-induced increase in sub-surface [H].[12]

We show that ambient exposure during the p-i interface preparation introduces silicon impurities into the interfacial region, presumably compensating Mg acceptors. In addition, the ex-situ dry etching improves the p-i interfacial crystallinity, but also introduces interfacial hydrogen.

Semiconductor devices are a cornerstone of modern device technology. Developing a better understanding of the process-structure-property relationship of these materials is critical for developing more efficient devices. If this relationship can be established, engineers responsible for

designing and growing these devices can make more informed decisions about their manufacturing processes, resulting in advancements in device design and quality. Our study can have a great value for III-V semiconductor and thin film growth communities.

Here, we present studies of the influence of p-i interface preparation on the structure and properties of p-i-n GaN heterostructures, prepared by metalorganic vapor-phase epitaxy (MOVPE) at Yale University, with and without ex-situ ambient exposure and/or ICP etching with Cl_2 and BCl_3 gas mixture. Each GaN p-i-n structure consists of a 350 nm thick layer of p-type Mg doped GaN (Mg ~ $0.5\times10^{21}/cm^3$) grown on a 1.5 μm thick layer of unintentionally doped (UID) GaN on a n-type GaN substrate. For "in-situ," the entire GaN p-i-n structure was grown without ambient exposure or dry etching. For "ex-situ," following the growth of the UID GaN layer, the sample was removed from the MOVPE chamber and experienced ambient exposure for one day prior to the re-insertion into the MOVPE chamber for growth of the p-type GaN layer. For "ICP-etched," the sample was also removed from the chamber following the growth of the UID GaN, and dry etching was conducted prior to re-insertion into the MOVPE chamber for the growth of the p-type GaN layer.

To study the [0001] channel environment and the fraction of displaced Ga atoms, we utilize H+ ions generated in the 1.7 MeV Tandem particle accelerator at the Michigan Ion Beam Laboratory, termed "Maize", which terminates in the Multi-Beam Chamber (MBC), that operates in the 10^{-7} Torr regime. Samples were mounted on the goniometer sample holder using conductive carbon tape. Within the MBC, the backscattered H+ were collected by a solid-state RBS detector situated at 160° with respect to the ion incident direction. For each sample, RBS spectra collected at the center of the [0001] channel provide the "aligned" yield. In addition, the goniometer is

randomly rotated in θ and ϕ (i.e. "rocked") from -5° to +5° about the [0001] channel to obtain the "unaligned" yield.

High resolution x-ray rocking curves HRXRC were collected in the Rigaku SmartLab using Cu Kα radiation conditioned by a 2-bounce Ge (220) monochromator. To probe the mosaic tilt and mosaic twist and subsequently quantify the densities of *c*- and *a*-type components of threading dislocations, we performed $\Delta\omega$ rocking curves about (0004) GaN and $\Delta\phi$ (azimuthal) scans about $(10\bar{1}5)$ GaN. The $\Delta\omega$ rocking curves were performed in a symmetric geometry, in which the angle, ω, between the incident beam and the sample surface is equal to the Bragg angle, θ_B, for a plane parallel to the sample surface. The incident beam is then "rocked" ± 0.3° about the Bragg angle. The $\Delta\phi$ scans are performed in an asymmetric geometry, where $\omega = \theta_B + \psi$, where ψ is the angle between the sample surface normal and the plane of interest normal. The sample is then rotated 0°-360° about the sample normal (ϕ-axis).

The depth-dependence concentrations of impurities were determined using a combination of secondary ion mass spectroscopy (SIMS) and Elastic Recoil Detection Analysis (ERDA). For ERDA, 2.5 MeV He+ ions were delivered at an angle of 70° to the sample surface normal, and recoiled H was collected by a solid-state detector situated at 30° with respect to the incident ion direction. Simultaneously, backscattered He+ was collected with the RBS detector situated at 170° with respect to the incident ion direction.

In preparation for SEM imaging and cathodoluminescence (CL) spectroscopy in the TESCAN RISE SEM, the samples were mounted film-side-up on planar SEM stubs using conductive carbon tape. CL emission was excited using 5 keV and 10 keV energy electrons, which are predicted by CASINO simulations to have maximum energy loss rates at 150 and 300 depth, thereby preferentially probing the p-GaN layer and the etched interface, respectively.[16] CL spectra

in the range 300-750 nm (4.13-1.65 eV) were collected with a Gatan MonoCL4 Plus system, in which a parabolic mirror focuses emitted photons into a Czerny-Turner monochromator (using the 1200 lines/mm diffraction grating), followed by a high sensitivity photomultiplier tube.[17]

Data:

The unaligned and aligned yield are normalized to the same total charge. The ratio of the aligned yield to the unaligned yield, termed the minimum yield min, is used to quantify the fraction of displaced Ga atoms, N_d/N, as follows:[18]

$$\frac{N_d}{N} = \frac{\chi_{min} - \chi_0}{1 - \chi_0} \tag{1}$$

where N is the atomic density of the crystal and χ_0 is the minimum yield for a high-quality GaN substrate. In **Fig. 1**, we present a comparison of the aligned and the unaligned RBS yields for the p-i-n GaN heterostructures. In the **Fig. 1 (a) (b)** and **(c)**, we present the normalized channeling RBS counts vs. Energy/depth for the GaN p-i-n structures, in comparison with that of the GaN substrate. Ga edge is apparent starting around 1.4 MeV, and N edge is apparent starting around 1.1 MeV. The “ICP-etched” GaN p-i-n structures have the lowest aligned yield at the Ga edge as well as the N edge. In the **Fig. 1 (d)**, we present fraction of displaced N atoms, $\frac{N_d}{N}$ (N), vs. depth. For all samples, the fraction of displaced N atoms, $\frac{N_d}{N}$ (N), is $<8\%$. It is interesting to note that the “in-situ” GaN p-i-n structure has the highest value of $\frac{N_d}{N}$ (N), and the “ICP-etched” GaN p-i-n structure has the lowest value of $\frac{N_d}{N}$ (N). In the **Fig. 1 (e)**, we present fraction of displaced Ga atoms, $\frac{N_d}{N}$, vs. depth. For all samples, the fraction of displaced Ga atoms, $\frac{N_d}{N}$ (Ga), is $<0.8\%$. It is interesting to

note that the "in-situ" GaN p-i-n structure has the highest value of $\frac{N_d}{N}$ (Ga), and the "ICP-etched" GaN p-i-n structure has the lowest value of $\frac{N_d}{N}$ (Ga).

Fig. 2(a) and **2(b)** show the (0004) $\Delta\omega$ rocking curves and $(10\bar{1}5)$ $\Delta\phi$ scans for the "In-situ", "Ex-situ", "ICP-etched", and GaN substrate. In **Fig. 2**, $\Delta\omega$ is plotted in arcsec (1° = 3600 arcsec) and $\Delta\phi$ is plotted in degrees. For both **Fig. 2(a)** and **2(b)**, the vertical axis is the log of the x-ray intensity. The widths of all x-ray rocking curves are quantified by the full width at half the maximum (FWHM), which are given in **Table 1**. In order to use the FWHMs to quantify the mosaic tilt and twist angles, all XRCs were fit using a Pseudo-Voigt function, which approximates the convolution of Cauchy C(x) and Gaussian G(x) profiles:

$$P(x) = I_0[\eta C(x) + (1-\eta)G(x)] \qquad 0 \le \eta \le 1 \tag{2}$$

where I_0 is the area under the curve and η is the Pseudo-Voigt fitting parameter that varies depending on the relative amounts of Cauchy or Gaussian character of the XRC profile. This model assumes profiles with relatively more Cauchy character ($\eta > 0.5$) result from small correlation lengths, whereas profiles with relatively more Gaussian character ($\eta < 0.5$) result from mosaic tilt.

The mosaic tilt angle, α_ω, is estimated as follows:[19]

$$\alpha_\omega = \beta_\omega[0.184446 + 0.812692(1-0.998497\eta)^{\frac{1}{2}} - 0.659603\eta + 0.44554\eta^2] \tag{3}$$

where β_ω is the full width at half the maximum (FWHM) of the $\Delta\omega$ rocking curve. The tilt angle is then used to estimate the density of *c*-type TD components, N_c, as follows:[20]

$$N_c = \frac{\alpha_\omega^2}{2\pi \boldsymbol{b}_c^2 ln2} \tag{4}$$

where $\boldsymbol{b}_c = [0001]$ is the Burgers vector for the *c*-type TD component where $|\boldsymbol{b}_c| = 0.5185$ nm. The lateral correlation length, $L_\parallel$, can also be estimated using α_ω and β_ω:[19]

$$L_\parallel = \frac{0.9\lambda}{\beta_\omega(0.017475+1.500484\eta-0.534156\eta^2)sin\theta_B} \tag{5}$$

where λ is the x-ray wavelength (λ = 1.541Å for Cu Kα_1) and θ_B is the Bragg angle. The density of a-type TD components, N_a, can then be estimated as follows:[20]

$$N_a = \frac{\alpha_\phi}{\sqrt{2\pi ln2}\,|\boldsymbol{b}_a| L_\parallel} \tag{6}$$

Where $\boldsymbol{b}_a = \frac{1}{3}\langle 11\bar{2}0\rangle$ is the Burgers vector for the a-type TD component where $|\boldsymbol{b}_a| = 0.3189$ nm and α_ϕ is the twist angle. Here, the twist angle is equal to the FWHM of the $\Delta\phi$ scan ($\alpha_\phi = \beta_\phi$). Eqn. (6) assumes that the a-type TDs are piled up at small angle grain boundaries, which results in a lower bound estimate for N_a. An upper bound estimate for N_a can be calculated assuming a random distribution of a-type TDs, but we do not make that assumption here.[19]

Table 1 gives the Pseudo Voigt fitting parameters, η, experimentally measured FWHMs, β_ω and $\beta_\phi = \alpha_\phi$, and the quantities calculated using Eqn. 3-6, α_ω, N_c, $L_\parallel$, N_a. For the $\Delta\omega$ rocking curves, all η values were < 0.5, suggesting that the $\Delta\omega$ peak broadening can be attributed to mosaic tilt in all samples. The two samples with ambient air exposure, the “Ex-situ” and “ICP-etched” samples, had the largest $\Delta\omega$ FWHM and largest tilt angles, resulting in the two highest N_c values. Overall, the “Ex-situ” had the largest N_c while the “In-situ” had the lowest. For the $\Delta\phi$ scans, the “In-situ” and “Ex-situ” samples had the largest $\Delta\phi$ FWHM/twist angles. However, the value of N_a for the “In-situ” sample is an order of magnitude larger compared to the other samples, all of which have very similar N_a values. Although the “In-situ” and “Ex-situ” samples both had the largest twist angles, the large lateral correlation length of the “Ex-situ” sample results in an N_a value similar to the “ICP-Etched” and GaN substrate.

To compute the effective depth-sensitivity of the electrons to the relevant impurities, we computed a convolution of the depth-dependence of the electron-induced excitation of free-electron-hole pairs with the depth-dependence of the areal impurity concentrations. The depth-dependence of the atomic concentrations for Si and Mg are determined by SIMS, while those for

H are determined by ERDA. The resulting depth-sensitivities of the electrons to Si, Mg, and H are shown in **Fig. 3 (a)**, **(b)**, and **(c)**, respectively. For all samples, the effective depth-sensitivity of Si is around 10^{16}. We noticed that for "Ex-situ" and "ICP-etched" samples, there is a peak in effective depth-sensitivity of Si around 350 nm where the p-i interface is located. The "ICP-etched" has the highest effective depth-sensitivity Si peak. For all samples, the effective depth-sensitivity of Mg is around 10^{19} form the surface to the 350 nm p-i interface and then drop to 10^{16}. For "ex-situ" and "ICP-etched" samples, we observed a peak of effective depth-sensitivity of Mg from 250 nm to 300 nm, where is near the p-i interface. The "ICP-etched" had a second peak around 350 nm. For all samples, we observed an enhancement of effective depth-sensitivity of H from 30 nm to 110 nm. We also noticed that only "ICP etched" samples had a peak of effective depth-sensitivity of H around 350 nm p-i interface.

In **Fig. 4**, the insert at the top left corner is a plot of CASINO Monte Carlo simulations of the energy loss rate, dE/dx, as a function of penetration depth for 5 and 10 keV electrons incident on GaN. As labeled in the CL spectra in both **Fig. 4 (a)** and **(b)**, CL emissions at 3.4 eV, 2.9 eV, and 2.2 eV are observed and attributed to the near-band-edge (NBE) excitonic emission, donor-acceptor pair (DAP) emission, and yellow luminescence (YL) emission, respectively.[21] For all GaN p-i-n structures, NBE and DAP emissions are apparent in both **Fig. 4 (a)** and **(b)**, indicating that both excitations likely occurred both within the p-GaN layer and at the p-i interface. Interestingly, YL emission is only observed in **Fig. 4 (b)** for the "ICP-etched" and "ex-situ" structures, suggesting that the YL is associated the ambient exposure of the p-i interface in those cases.

The "in-situ" has the highest DAP and NBE emissions at its surface and interface, respectively. For "ex-situ" the intensity for DAP and NBE does not change between surface and

interface. For "ICP-etched", the DAP and NBE enhance from surface to interface. We also noticed that the trend in N_c mirrored the trend of the DAP emissions at the interface, with the "in-situ" having the lowest N_c, followed by "ICP-etched", followed by "Ex-situ", which has the highest N_c. The intensities of the DAP emissions at the p-i interface follow the reverse trend, where "Ex-situ" has the lowest DAP emission, followed by "ICP-etched", and "In-situ" having the highest DAP emission.

YL emission is attributed to the transition from shallow donor levels to deep acceptor centers, either V_{Ga}-O_N (gallium-vacancy-oxygen-on-nitrogen-site), [22, 23] or V_{Ga}-Si_{Ga} (gallium-vacancy-silicon on gallium site).[16, 17] The enhanced [Si] seen in the SIMS data at the p-i interfaces of the "ex-situ" and "ICP-etched" structures, along with the presence YL emission at the p-i interface for both the "ex-situ" and the "ICP-etched" structures, indicates the presence of V_{Ga}-Si_{Ga} defect complexes at the p-i interface. Similarly, the absence of YL emission for the "in-situ" structure suggests the absence of V_{Ga}-Si_{Ga} defect complexes. Thus, the YL emission at the p-i interface of the "ex-situ" and the "ICP-etched" structures indicates that the ambient exposure step of the GaN p-i-n structure preparation is associated with the introduction of silicon impurities.

To summarize, we noticed that the "ICP-etched" and "ex-situ" GaN p-i-n structure have the similar value of $\frac{N_d}{N}$ (Ga) and $\frac{N_d}{N}$ (N) at the regrown interface (~350 nm), while the "in-situ" GaN p-i-n structure has the highest value of $\frac{N_d}{N}$ (Ga) and $\frac{N_d}{N}$ (N) at the regrown interface. "In-situ" has the highest N_a (a-type TD) and lowest N_c (c-type TD), and "ex-situ" has the highest N_c. At the regrown interface, the effective depth-sensitivities for Si, Mg, and H are highest for ICP-etched. Near the regrown interface, the effective depth-sensitivities for Mg, and Si are enhanced for Ex-situ. DAP emission for ICP-etched is enhanced at the regrown interface. DAP emissions are higher for in-situ than for ex-situ both in the regrown layer and at the regrown interface. The trend in N_c

mirrors the trend of the DAP emissions at the interface, with the "in-situ" having the lowest N_c and highest DAP, followed by "ICP-etched", followed by "Ex-situ", which has the highest N_c and lowest DAP. YL emission at the p-i interface for both the "ex-situ" and the "ICP-etched" structures, indicates the presence of V_{Ga}-Si_{Ga} defect complexes at the p-i interface. Similarly, the absence of YL emission for the "in-situ" structure suggests the absence of V_{Ga}-Si_{Ga} defect complexes. Thus, the YL emission at the p-i interface of the "ex-situ" and the "ICP-etched" structures indicates that the ambient exposure step of the GaN p-i-n structure preparation is associated with the introduction of silicon impurities.

We hypothesize *c*-type dislocations decrease DAP and NBE, but excess Si, Mg, & H at interface increase DAP and NBE. We also hypothesize that for "ex-situ" and "ICP-etched", the Si at the regrown interface suppress the activation of the Mg. For "ICP-etched", the H at the interface help the activation of the Mg and compensate the DAP emission. "ICP-etched" is an ex-situ process, but unlike the untreated "ex-situ", the electronic properties are partially restored to be comparable with the "in-situ". This demonstrates that ex-situ growth with some treatment has the potential to have the growth interface properties comparable to that using in-situ growth condition.

SUPPLEMENTAL MATERIALS

See the supplemental materials for ERDA and SIMS data, as well as the computed values of the energy loss rate, dE/dx, as a function of penetration depth for 5 and 10 keV electrons.

ACKNOWLEDGEMENTS

We gratefully acknowledge support from the ARPA-E AED0000191 and the Michigan Ion Beam Laboratory.

FIGURES AND TABLES

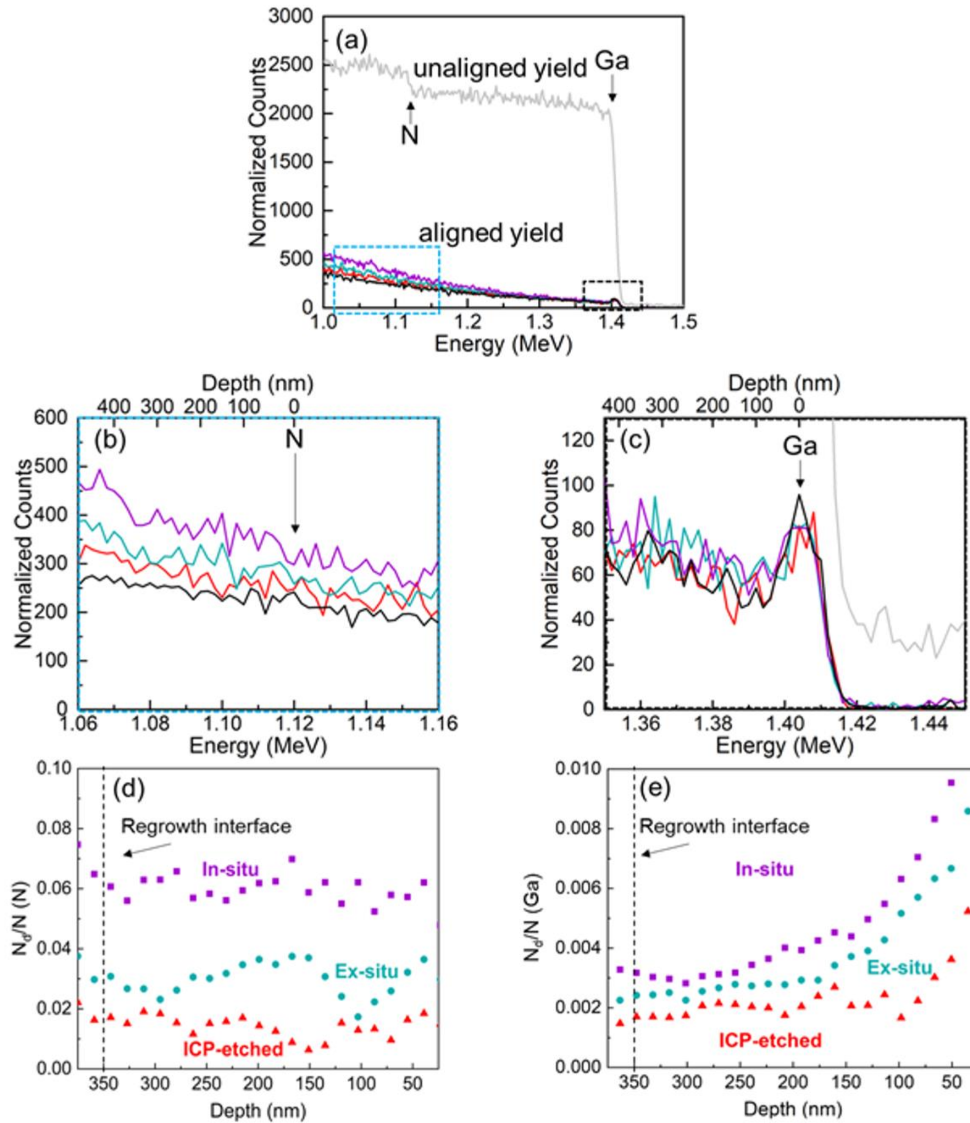

FIG. 1: (a) Normalized channeling Rutherford Backscattering Spectroscopy (RBS) counts vs. Energy/depth for the GaN p-i-n structures, in comparison with that of the GaN substrate. The unaligned normalized yield spectrum is shown as a grey line. The aligned normalized yields for the substrate, "in-situ," "ex-situ," "etched," GaN p-i-n structures are shown in black, purple, green, and red, respectively. The portions of the RBS spectra enclosed in the blue box in (a), the N edge, are shown in (b). The portions of the RBS spectra enclosed in the black box in (a), the Ga edge, are shown in (c). The "etched" GaN p-i-n structures have the lowest aligned yields at the Ga edge

and the N edge. (d) Fraction of displaced N atoms, N_d/N (N), vs. depth for “in-situ”, “ex-situ” and “etched” GaN p-i-n structures. The fraction of displaced N atoms is also the lowest for the “etched” GaN p-i-n structure. (e) Fraction of displaced Ga atoms, N_d/N (Ga), vs. depth for “in-situ”, “ex-situ” and “etched” GaN p-i-n structures. The fraction of displaced Ga atoms is the lowest for the “etched” GaN p-i-n structure.

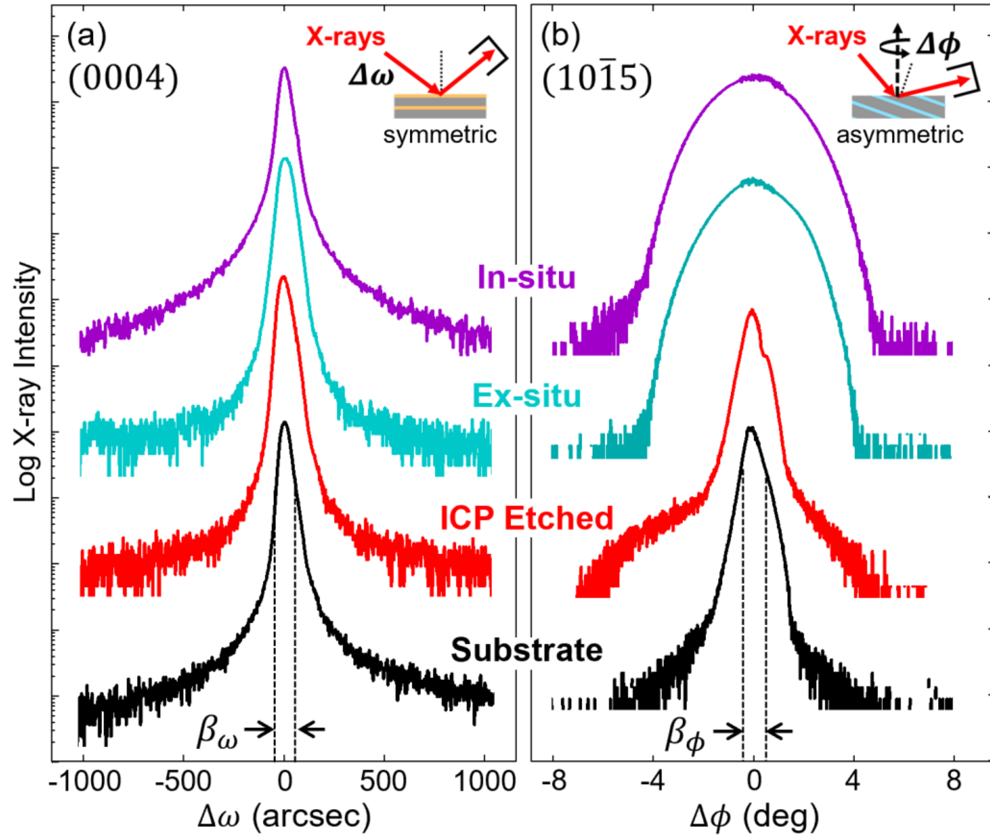

FIG. 2: X-ray rocking curves for the (a) symmetric (0004) $\Delta\omega$ scans and (b) asymmetric $(10\bar{1}5)$ $\Delta\phi$ scans for the GaN substrate and the "in-situ", "ex-situ" and "etched" GaN p-i-n structures. The FWHM of the $\Delta\omega$ and $\Delta\phi$ scans, $\delta\omega$ and $\delta\phi$, are used to estimate the densities of the *c*-type and *a*-type components of TDs, respectively, according to methods of Metzger et al. The "in-situ" has the lowest density of *c*-type and largest density of *a*-type TD components.

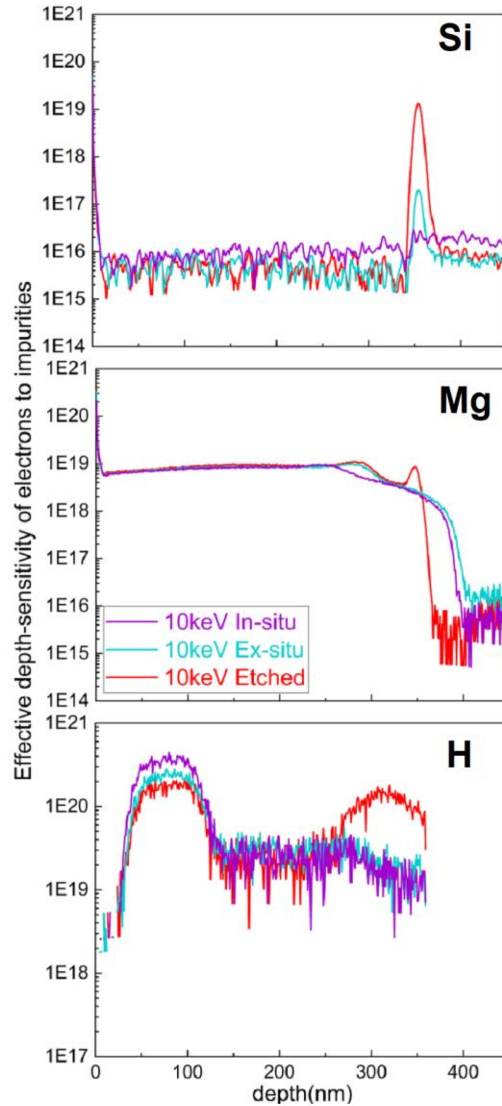

FIG. 3: Effective depth-sensitivity of electrons to impurities. Convolution of depth-dependent electron-induced excitation of free-electron-hole pairs with depth-dependent areal impurity concentrations. The depth-dependence of electron-induced excitations were computed using a CASINO Monte Carlo simulation of energy loss rates. The depth-dependence of the areal impurity concentrations were determined using secondary ion mass spectrometry (for Si and Mg) and elastic recoil detection analysis (for H). For the Ex-situ sample, the effective depth-sensitivity for Si is enhanced at the p-i interface. For ICP-etched sample, the effective depth-sensitivity for Si, Mg, and H are enhanced at the p-i interface.

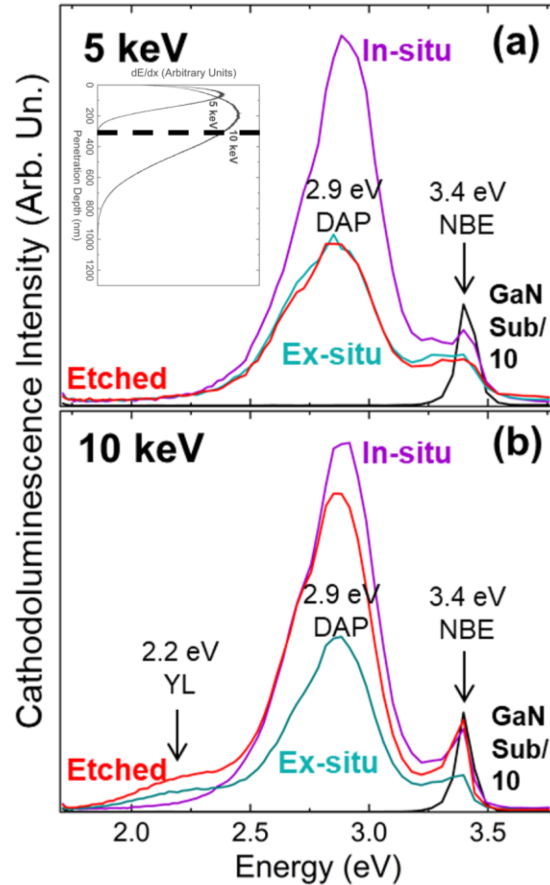

FIG. 4: Cathodoluminescence intensity vs. Energy for “in-situ,” “ex-situ,” and “ICP-etched” regrown GaN (a) 5 keV and (b) 10 keV incident electrons. The electron penetration depths reveal that 5 keV electrons probe the near-surface region and the 10 keV electrons probe the p-i interface region. For all GaN p-i-n structures, the donor-acceptor pair (DAP) and near-band-edge (NBE) emissions are observed at both the near-surface and the interface regions, while the GaN substrate (not shown) exhibits only the NBE emission. Interestingly, DAP emissions are highest for the “in-situ” interface; and highest NBE and yellow luminescence (YL) emissions are highest for the “ICP-etched” interface.

Sample	β_ω (arcsec)	η (from $\Delta\omega$)	α_ω (10^{-4} rad)	$\boldsymbol{N_c}$ (10^6 cm^{-2})	$L_\parallel$ (μm)	$\beta_\phi = \alpha_\phi$ (10^{-4} rad)	$\boldsymbol{N_a}$ (10^8 cm^{-2})
In-situ	52	0.428	1.5	**1.9**	1.7	528	**47.5**
Ex-situ	68	0.033	3.2	**8.6**	11	454	**6.4**
ICP Etched	59	0.229	2.2	**4.2**	2.4	102	**6.2**
Substrate	50	0.222	1.9	**3.1**	3.0	108	**6.3**

Table. 1: The measured values for the (0004) $\Delta\omega$ FWHM (β_ω), Pseudo Voigt fitting parameter (η), $(10\bar{1}5)$ $\Delta\phi$ FWHM (β_ϕ), and the twist angle (α_ϕ), and the calculated values for the tilt angle (α_ω), lateral correlation length ($L_\parallel$), c-type TD density (N_c), and a-type TD density (N_a).

[1] R. Yeluri, J. Lu, C. A. Hurni, D. A. Browne, S. Chowdhury, S. Keller, J. S. Speck, U. K. Mishra, “Design, Fabrication, and Performance Analysis of GaN Vertical Electron Transistors with a Buried P/N Junction,” Appl. Phys. Lett., vol. 106, p. 183502 (2015).

[2] Y. Zhang, M. Sun, Z. Liu, D. Piedra, H.-S. Lee, F. Gao, T. Fujishima, T. Palacios, “Electrothermal Simulation and Thermal Performance Study of GaN Vertical and Lateral Power Transistors,” IEEE Trans. Electron Devices, vol. 60, p. 2224-2230 (2013).

[3] T. Uesugi, T. Kachi, “Which Are the Future GaN Power Devices for Automotive Applications, Lateral Structures or Vertical Structures?” CS Mantech Conference, Toyota Central R&D Laboratories, 1-4 (2011).

[4] B. Li, M. Nami, S. Wang, J. Han, “In-situ and Selective Area Etching of GaN by Tertiary-butyl-chloride (TBCl),” Appl. Phys. Lett. vol. 115, p. 162101 (2019).

[5] J. D. Greenlee, B. N. Feigelson, T. J. Anderson, J. K. Hite, K. D. Hobart, and F. J. Kub. “Symmetric Multicycle Rapid Thermal Annealing: Enhanced Activation of Implanted Dopants in GaN,” ECS J. Solid State Sci. Technol. vol. 4, p. 382-386 (2015).

[6] K. Kojima, S. Takashima, M. Edo, K. Ueno, M. Shimizu, T. Takahashi, S. Ishibashi, A. Uedono, and S. F. Chichibu. “Nitrogen Vacancies as a Common Element of the Green Luminescence and Nonradiative Recombination Centers in Mg-Implanted GaN layers Formed on a GaN Substrate,” Appl. Phys. Express vol. 10, p. 061002 (2017).

[7] H. Liu, H. Fu, K. Fu, S. Algubelli, P. S, Y. Zhao, F. Ponce. “Non-uniform Mg distribution in GaN Epilayers Grown on Mesa Structures for Applications in GaN Power Electronics,” Appl. Phys. Lett. vol. 114, p. 082102 (2019).

[8] N. Asai, H. Ohta, F. Horikiri, Y. Narita, T. Yoshida, T. Mishima. “Impact of Damage-free Wet Etching Process in Fabrication of High Breakdown Voltage GaN p-n Junction,” Jpn. J. Appl. Phys. vol. 58, SCCD05 (2019).

[9] Q. Fan, S. Chevtchenko, X. Ni, S. Cho, F. Yun, H. Morkoc, “Reactive Ion Etch Damage on GaN and its Recovery,” Journal of Vacuum Science & Technology B, vol. 24, p. 1197 (2006)

[10] A. Aragon, M. Monavarian, I. Stricklin, G. Pickrell, M. Crawford, A. Allerman, A. Armstrong, D. Feezell, “Interfacial Impurities and Their Electronic Signatures in High-Voltage Regrown Non-planar m-plane GaN vertical p-n diodes,” Phys. Status. Solidi A, 217: 1900757 (2019)

[11] M. Xiao, X. Yan, J. Xie, E. Beam, Y. Cao, H. Wang, Y. Zhang, “Origin of leakage current in vertical GaN devices with non-planar regrown GaN,” Appl. Phys. Lett, 117, 183502 (2020)

[12] J. Kennedy, A. Markwitz, H.J. Trodahl, B.J. Ruck, S.M. Durbin, and W. Gao, “Ion Beam Analysis of Amorphous and Nanocrystalline Group III-V Nitride and ZnO Thin Films”, Journal of Electronic Materials vol. 36, p. 472 (2007).

[13] U. Muhammad, H. Anders, N. Aftab, “Ion Implantation Induced Nitrogen Defects in GaN,” J. Phys. D: Appl. Phys. vol. 48, p. 45(2015).

[14] N. Nishikata, K. Kushida, T. Nishimura, T. Mishima, K. Kuriyama, and T. Nakamura, “Evaluation of Lattice Displacement in Mg-Implanted GaN by Rutherford Backscattering Spectroscopy” Nuclear Instruments and Methods in Physics Research Section B: Beam Interactions with Materials and Atoms, vol. 409, p. 302-304 (2017).

[15] A. Redondo-Cubero, K. Lorenz, R. Gago, N. Franco, S. Fernández-Garrido, P.J.M. Smulders, E. Muñoz, E. Calleja, I.M. Watson, and E. Alves, “Breakdown of Anomalous Channeling with Ion Energy for Accurate Strain Determination in GaN-based Heterostructures.” Applied Physics Letters vol. 95, p. 051921 (2009).

[16] [Supplemental material reference]

[17] [MonoCL4 manual or similar]

[18] W.K. Chu, J.W. Mayer, M.A. Nicolet, in: Backscattering Spectrometry, Academic, New York, 1978 (Chapter 8).

[19] T. Metzger, R. Höpler, E. Born, O. Ambacher, M. Stutzmann, R. Stömmer, M. Schuster, H. Göbel, S. Christiansen, M. Albrecht, H.P. Strunk, "Defect structure of epitaxial GaN films determined by transmission electron microscopy and triple-axis X-ray diffractometry." Philosophical Magazine A vol. 77, p. 1013-1025 (1998).

[20] M. Frentrup, L. Y. Lee, S. L. Sahonta, M. J. Kappers, F. Massabuau, P. Gupta, R. A. Oliver, C. J. Humphreys, D. J. Wallis, "X-ray diffraction analysis of cubic zincblende III-nitrides." J. Phys. D: Appl. Phys. vol. 50, p. 433002 (2017).

[21] M. Hopstaken, M. Gordon, D. Pfeiffer, D. Sadana, T. Topuria, P. Rice, C. Gerl, M. Richter, C. Marchiori, "Sputtering Behavior and Evolution of Depth Resolution upon Low Energy Ion Irradiation of GaAs," Vac. Sci. & Tech. B. p. 207-215 (2010).

[22] U. Kaufmann, M. Kunzer, M. Maier, H. Obloh, A. Ramakrishnan, B. Santic, P. Schlotter "Nature of the 2.8 eV Photoluminescence Band in Mg Doped GaN," Appl. Phys. Lett. vol. 72, p. 1326, (1998).

[23] M. Matys, M. Miczek, B. Adamowicz, Z.R. Zytkiewicz, E. Kaminska, A. Piotrowska, T. Hashizume, "The Impact of Bulk Defects, Surface States, and Excitons on Yellow and Ultraviolet Photoluminescence in GaN," Acta Physica Polonica A, vol. 120, p. 73-75 (2011).